Study and Modeling of the Grinding Kinetics of Reactive Rocks in a Cement Laboratory

Seke Vangu Max[1,2]* [ID], **Pongo Pongo Charles[3]** [ID], **Pongo Pongo Kalang Hochéà[1]** [ID],
Musuamba Kabengele Nathalie[1] [ID], **Kisonga Manuku Eric[1]**,
Mungyeko Bisulandu Baby-Jean Robert[4] [ID]

[1]Faculté des sciences et technologies, Université de Kinshasa, Kinshasa, Democratic Republic of the Congo
[2]Faculté Polytechnique, Université Kongo, Mbanza-Ngungu, Democratic Republic of the Congo
[3]Pretoria Portland Cement, Quality Assurance, Malanga, Democratic Republic of the Congo
[4]Institut de Recherche Futuris—Futuris Research Institute (InReF), OEFC & Département de Génie Rural, Institut National du Bâtiment et des Travaux Publics (INBTP), Kinshasa, Democratic Republic of the Congo
Email: *max.seke@unikin.ac.cd

Abstract

This article focuses on the study of crushing rocks that can replace clinker in low-carbon cement. A laboratory ball mill was used, varying the duration of the grinding. It has been observed that the specific surface of rocks changes in a nonlinear way with time, due to the agglomeration of particles. To this end, a mathematical model describing this evolution, which considers van der Waals forces, has been proposed. And finally, the model was adjusted regarding the experimental data. The results found show that the present model is more accurate than the classical models, because it considers the agglomeration phenomenon.

Keywords

Cementitious Materials, Blaine, Grindability, Modeling, Rittinger, Van Der Waals

1. Introduction

Grinding modifies the specific surface, the particle size distribution, and the morphology of the particles, which have an impact on the physicochemical and mechanical properties of the materials. In the cement industry, grinding fineness is an essential criterion that conditions and characterizes the quality of the final product. The real-time evaluation of this fineness is an important parameter of a grinder, which requires prediction using reliable mathematical models, consi-

dered as key elements to ensure the quality parameters of the product while optimizing the energy efficiency. Grinding aims to prepare the ground material to achieve a grinding fineness suitable for specific applications. This fineness is usually expressed in terms of Blaine-specific surface and percentage of rejection at the 45-micron sieve. The physical and chemical properties of the material are closely related to the grinding fineness obtained, an important parameter that can significantly affect the performance of the final product [1] [2] [3].

The literature proposes models for the grinding of materials and their key parameters [4]-[12]. These authors consider the factors that influence the grinding (type of material, grinder, operating conditions, interactions between particles). Some authors report that the agglomeration of fine particles, due to van der Waals or electrostatic forces [13] [14] [15] [16] [17], leads to the decrease of the specific surface and consequently the increase of the energy consumption and the modification of the product properties. Blanc *et al.* [18] analyzed the long-term grinding of silica sand in an oscillating ball mill. They highlighted the correlation between the agglomeration of fine particles and the volume fraction of the finest ones, which influences the specific surface as a function of grinding time. They developed a nonlinear comminution model that modifies Rittinger's law with a term function of the volume fraction of the finest ones. They fitted the model to the experimental data, and they confirmed its ability to reproduce the specific surface as a function of grinding time.

Yang *et al.* [19] studied polymer-based additions to improve the grindability of cement. They showed that the polymer-based grinding aid increases the specific surface, prevents agglomeration and ball coatings, and improves the roundness, fineness and fluidity of the ground cement. Ghalandari and Iranmanesh [20] analyzed the energy and exergy of a cement ball mill to improve the grinding efficiency. According to Katsioti et al. [21] [22], grinding additives influence the grindability of cement, as they showed by spectroscopic and chromatographic techniques. Toprak *et al.* [23] [24] also studied the effect of grinding additives on the grinding and fineness of cement, considering the material transport in the mill. Zunino and Scrivener [25] used alkanol amines as grinding aids to reduce the agglomeration of cement particles. This paper compares the grinding kinetics of rocks from Kongo Central [26] and an industrial clinker in a laboratory ball mill. We measure the specific surface as a function of grinding time. We model the specific surface by nonlinear functions and propose a mathematical model descriptive of the grinding phenomenon. We analyse the effects of agglomeration on individual grinding and suggest strategies to mitigate or avoid it, to improve the efficiency and quality of the process. The agglomeration of particles in cement ball mills is influenced by inter-particle forces, which vary with particle sizes. Giraud [27] proposed a diagram illustrating the attraction and adhesion forces of masses as a function of particle diameters, which allows to explain the agglomeration mechanisms in a ball mill.

The efficiency of cement ball mills without additives is limited by the re-agglo-

meration of fine particles and the coating of grinding media, which hinder the achievement of optimal powder fineness, even by increasing the grinding time [28]. To analyze this problem on different types of rocks, it is necessary to determine the optimal grinding time that allows it to reach a maximum specific surface and to examine the possible solutions to improve the process. A possible approach is to model the grinding kinetics of the granular system [29] [30]. In this paper, we propose several mathematical models to describe the dry micronization kinetics of various rocks in a laboratory ball mill. The objective is to better understand the Van der Waals interactions within a granular system, such as a rock undergoing micronization, as well as the origin and prediction of the agglomeration phenomenon [31] [32]. This study can have practical implications for the industry, by facilitating the understanding of the grinding mechanisms and the use of grinding aids [33] [34]. This contribution is relevant both academically and industrially. Chodakov [35] [36] established a mathematical relationship between the specific surface, the maximum specific surface, the grinding constant and the grinding time. Opoczky [37] [38] distinguished three grinding regions: the Rittinger region where energy is proportional to the creation of new surfaces without intra-particle interactions, the aggregation region where inter-particle interactions are governed by cohesive Van der Waals forces and break linearity, and the agglomeration region where performance decreases with fineness. These models are useful academically and industrially, as they help to understand and optimize the grinding of granular systems [33] [37] [39].

Gabor Mucsi *et al.* [39] [40] showed that the specific surface increases rapidly, then more slowly, and reaches a maximum, indicating the saturation of grinding. The additional energy lowers the Blaine. The agglomeration and aggregation of rock particles are explained by the van der Waals forces between the molecules, which form inter-particle bonds that are difficult to break during grinding [41]. These forces are short-range electrostatic interactions due to fluctuations in the charge density of the particles. They are weaker than covalent or ionic bonds, but they are important in many fields such as supramolecular chemistry, structural biology, polymer science, nanotechnology, surface science and condensed matter physics [42] [43]. The van der Waals forces influence the grinding by promoting or hindering the agglomeration and aggregation of particles depending on the characteristics of the ground materials, the particle size, the temperature, and the grinding conditions [44]. These phenomena affect the grindability of clinker, *i.e.* its ease to be reduced to fine powder. The grindability of clinker also depends on its chemical and mineralogical composition. Unland *et al.* [45] [46] proved that the grindability of clinker improves with alite and degrades with belite. Therefore, these factors must be considered to design high-quality cements, optimize the production process and minimize the energy consumption required for grinding.

2. Materials and Methods

In this part, we present the materials and methods for the grinding monitoring

of the three reactive rocks in a cement laboratory as well as the clinker. A description of the rocks is given, as well as the grinding, the measurements of the specific surface and the fineness of the powders, and the chemical and mineralogical analyses. We also explain the mathematical models to fit the data and evaluate the kinetic parameters.

2.1. The Rocks of Study

The rocks studied in this article are semi-finished materials, which can be used as substitutes or additives in the manufacture of cement. They are clinker with high belite content, as well as basalt, metabasalt and dolerite. The chemical (mineralogical) compositions of these rocks (Dolertite, Basalt and Metabasalt) were determined by X-ray diffraction technique and are presented in **Table 1** and **Table 2**.

Table 1 presents the chemical compositions (in oxides) of the rocks under investigation. The SiO_2 and Al_2O_3 content ranges from 56.96% for the dolerite to 63.5% for the metabasalt, with 60.69% for the basalt in between. These oxides form covalent bonds, which are harder to break than ionic bonds [48]-[53].

Therefore, the dolerite should be less crushable than the basalt, whereas the metabasalt should be the most crushable according to this criterion. **Table 2** presents the mineralogical composition of the rocks under investigation, determined by the X-ray diffraction technique. It is noted that the basalt mainly consists of plagioclases, pyroxenes and olivine, that the dolerite is dominated by amphiboles and biotite, and that the metabasalt mostly comprises epidote and quartz. The relative proportions of these minerals can affect the physical and

Table 1. X-ray fluorescence analysis of three geomaterials under investigation [47].

	Dol.	Bas.	Meta.
SiO_2	44.44	46.25	49.3
Al_2O_3	12.52	14.44	14.2
Fe_2O_3	16.18	15.85	12.7
CaO	11.27	8.86	15.7
Na_2O	2.46	4.4	0
K_2O	0.79	0.33	0.14
TiO_2	1.98	2.29	0.91
MnO	0	0.15	0
P_2O_5	0.19	0.31	0.15
MgO	7.33	3.44	3.05
SO_3	0.25	0.23	0.03
P. F	2.83	3.65	2.05
$K_2O + Na_2O$	*3.25*	*4.73*	*0.14*

Table 2. X-ray diffraction mineralogy of three geomaterials under study [47] and computed Mohs hardness.

Minerals	Bas.	Dol.	Meta.
Albite	24.53	5.96	3.86
Anorthite	28.73	7.15	0
Diopside	7.68	0	6.32
Biotite	0	7.05	0.96
Olivine	1.56	0	0
Chlorite	19.56	28.96	3.24
Amphibole	2.62	33.46	9.73
Hypersthene	13.2	0	1.28
Quartz	0.98	6.93	23.56
Orthoses	3.14	0	8.22
Epidote	0	10.49	42.83

mechanical properties of the rocks, as well as their suitability for various industrial applications. Albite and orthoclase are silicate minerals, which can enhance their reactivity with lime and improve the performance of cement. For the clinker, the results of its mineralogy are provided in Table 3.

Table 3 shows the mineralogical composition of the clinker used in this article, determined by the X-ray diffraction technique. The clinker is essentially composed of two mineral phases: tricalcium silicate (C_3S) and dicalcium silicate (C_2S), which account for 34.1% and 40.1% of the total mass, respectively. The clinker also contains tricalcium aluminate (C3A) and tetracalcium ferroaluminate (C_4AF), but in lower proportions (9.1% and 14.7%, respectively). Other minerals are present in traces in the clinker, such as arcanite (K_2SO_4), langbeinite ($K_2Mg_2(SO_4)_3$), portlandite ($Ca(OH)_2$), quartz (SiO_2) and aphthitalite ($K_3Na(SO_4)_2$), as well as free lime (CaO) and periclase (MgO).

2.2. Jaw Crusher

The crusher used in this article is a jaw crusher Figure 1, which works by compressing the aggregates between two steel plates, one fixed and the other movable. The steel plates are coated with a wear-resistant material and can be adjusted to control the size of the crushed products. The crusher is fed by a hopper that dumps the aggregates into the crushing chamber formed by the steel plates [56] [57]. This crusher complies with the standard (EN 349:1993) on machine safety. This equipment allows to reduce the size of the aggregates to less than 7 mm, in accordance with the requirements of the ball mill grindability test, whose characteristics are presented in Table 4 and Table 5.

Table 3. X-ray diffraction mineralogy of clinker under investigation [26] and computed Mohs hardness.

| Minéraux Clinker	Taux %	Dureté Mohs
C_3S	34.1	4.5
C_2S	40.1	6
C_3A	9.1	6
C_4AF	14.7	5.5
Arcanite	0.1	3
Langbeinite	0.6	3.5
Portlandite	0.2	2.5
Free Lime	3.9	
Periclase	0.6	6
Aphtitalite	0.3	3
Quartz	0.2	7

Table 4. Shapes, dimensions and quantity of Grinding media.

Name	Diameter	Q'ty (pc)	Weight	Picture
Steel Ball	40	43	60	
	50	37		
	60	24		
	70	9		
Wroght Steel	D	374	40	
	$\dfrac{mm*L(mm)}{25*30}$			

Table 5. Specifications of the Mill elements (SM-500).

|	
Diameter & length (internal)	500 * 500 mm^2
Mass of Grinding media	100 kg
Maximum grain size	7 mm
Loading capacity	≤5 kg
Rotation speed	≈48 r/min
Grinding time	≈30 min
Net weight of the machine	≈300 kg
Motor power	1.5 KW
Voltage	220 V/380V
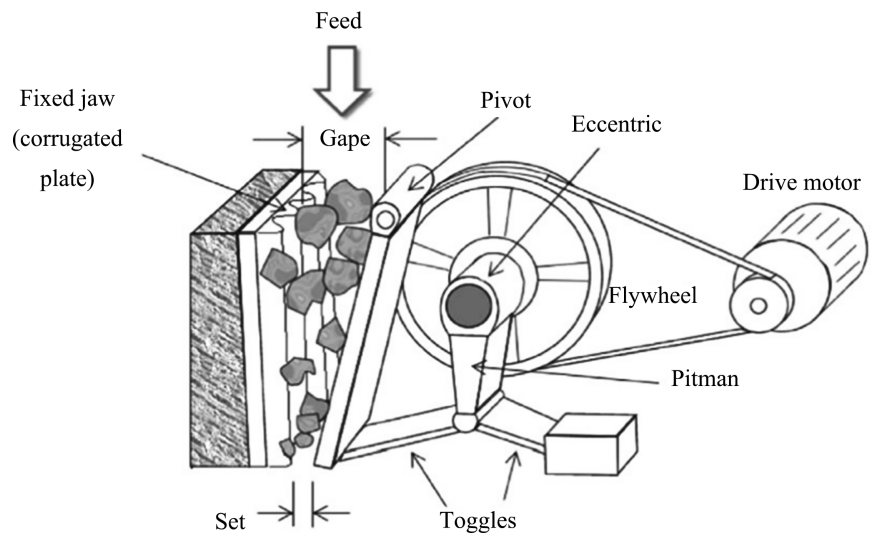
Figure 1. Schematic of a jaw crusher [54] [55].

2.3. Laboratory Ball Mill

The pilot-scale ball mill is used to study and analyze the grinding process of these rocks. **Table 4** and **Table 5** show the dimensions of the grinding media (balls), as well as other characteristics.

The ball mill used in this article is the SM-500 model from the Cement Test Mill brand. It is a laboratory mill consisting of a horizontal cylindrical drum of 500 mm in diameter and length, filled with 100 kg of steel balls. This mill can process 5 kg of rocks per cycle, which corresponds to a loading ratio of 20. The mill uses balls of different sizes and shapes, in order to create an optimal arrangement of balls in the drum, which maximizes the contact surface with the rocks and minimizes the void spaces between the balls [41]. This method allows to optimize the grinding performance, by reducing the time required to reach the required fineness, as well as the associated energy consumption [58]. The technical characteristics of the mill are summarized in **Table 4** and **Table 5**.

The ball mill grinding depends on the rotation speed of the drum, which can be classified into three regimes: cascade, cataract and centrifugation. **Figure 2** schematizes these regimes. The cascade regime, which corresponds to a low rotation speed, induces friction between the balls and the wall of the drum, which is inefficient for grinding. The centrifugation regime, which corresponds to a rotation speed higher than the critical speed, causes the adhesion of the balls to the wall of the drum, which is also inefficient for grinding. The cataract regime, which corresponds to an intermediate rotation speed, involves a movement of the balls in free fall, which generates impacts between the balls and the particles to be ground. This regime is the most efficient for grinding hard materials.

The critical speed of the mill is defined as the minimum speed at which the balls are driven by the centrifugal force without falling. It depends on the internal diameter of the drum and can be calculated by the following formula: $V_{critical} = 42.4/(D_i)^{0.5}$ where $V_{critical}$ is expressed in m/s and D_i in m. The cataract

(a)   (b)   (c)
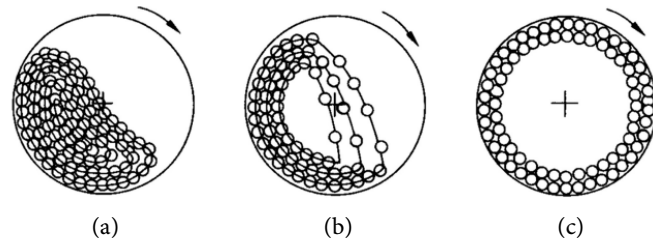
Figure 2. Rotation (a) Mode cascade (b) Mode cataracte (c) centrifugal mode [59] [60].

speed of the mill is defined as the optimal speed at which the balls move in cataract, *i.e.* they are lifted up to a certain height and then fall freely. It depends on the diameter and mass of the balls and can be estimated by multiplying the critical speed by a cataract coefficient, usually between 0.6 and 0.8. A commonly used value for the cataract coefficient is 0.75 [61]. Thus, the cataract speed can be calculated by the following formula: Vcataract = 0.75 * V$_{critical}$. This correlation produces **Table 6**.

The critical rotation speed of the drum as a function of the diameter in cataract and critical modes is represented in **Figure 3**.

2.4. Automatic Blaine Meter

The measurement of the grinding fineness or grindability is done with a Blaine measurement device as shown in **Figure 4**.

The grindability was evaluated at regular time intervals (5 to 10 minutes) using the Blaine method, which consists of measuring the air permeability of a compacted powder bed according to the European standard **(EN 196-6)**. The specific surface area of the powders was calculated from the permeability by applying the Blaine formula, which establishes a relationship between these two parameters [62] [63].

2.5. A Matlab/Simulink R2020b

Matlab/Simulink R2020b software with its Curve Fitting Tool library to plot and fit the experimental points "Blaine (cm^2/g) vs. Grinding time (min)". This study selected four mathematical models: the logarithmic model (Modified Rittinger), the logistic model, the quadratic polynomial model and the two-component exponential model. The corresponding equations are summarized in **Table 7**.

The constants and statistical parameters R^2, RMSE and SSE of the four models were calculated using the Matlab tool. These criteria were used to select the best model for each rock. The constants of the models have the following physical meanings.

2.5.1. Logistic Model: $A_1 \big/ \left(A_0 \mathrm{e}^{-k_0 \cdot t} + 1 \right) = L \big/ \left(1 + \mathrm{e}^{-k_0 (t - t_0)} \right)$

For the logistic model, $L = A_1$ represents the asymptotic limit of the Blaine, $k = k_0$ represents the maximum growth rate that determines the speed at which the logistic curve reaches its upper limit. This constant depends on the hardness of
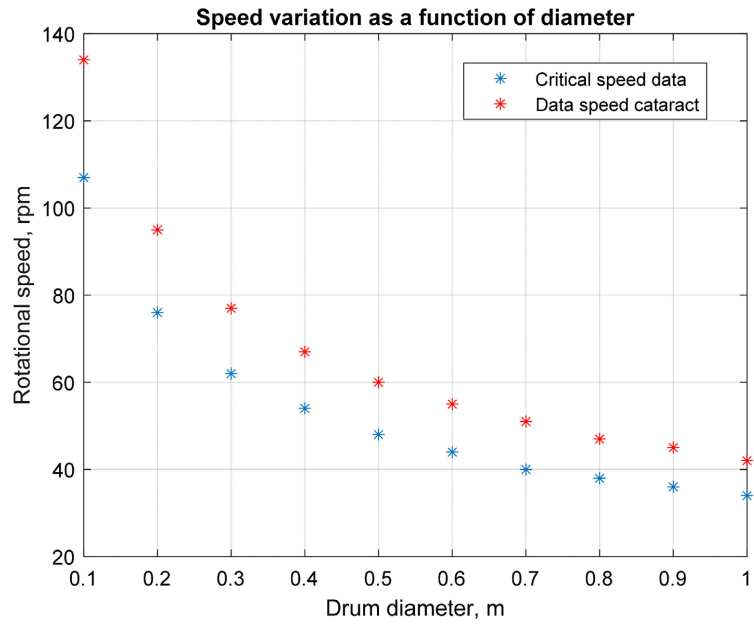
Figure 3. Graphical representation of the speed as a function of the internal diameter of the drum.

Figure 4. Device for the specific surface.

Table 6. Critical rotation speed of the drum as a function of the diameter and the cataract coefficient.

D (m)	$42.3/D^{0.5}$ Critical (rpm)	$V_{cataract}$ (rpm)
0.1	134	107
0.2	95	76
0.3	77	62
0.4	67	54
0.5	60	48
0.6	55	44
0.7	51	40
0.8	47	38
0.9	45	36
1	42	34

Table 7. Presentation of mathematical models to describe the kinetics.

Modèle-1. Logarithmique	$A_0 \mathrm{e}^{-k*t} + A_1 = a\left(1 - b\mathrm{e}^{-c*t}\right)$
Modèle-2. Logistique	$A_1 \big/ \left(A_0 * \mathrm{e}^{-k_0 *t} + 1\right) = L \big/ \left(1 + \mathrm{e}^{-k(t-t_0)}\right)$
Modèle-3. Quadratique	$A_2 t^2 + A_1 t + A_0 = a + bt + ct^2$
Modèle-4. Exponentiel-2	$A_0 \mathrm{e}^{-k_0 *t} + A_1 \mathrm{e}^{-k_1 *t} = a + b\left(1 - \mathrm{e}^{-c*t}\right) + d\left(1 - \mathrm{e}^{-e*t}\right)$

the rock, the energy provided by the mill and the operating conditions (temperature, pressure…). A higher k constant corresponds to a faster increase in the fineness of the powder. Constant t_0 represents the time required to reach half of the asymptotic value of the Blaine. $A_0 = \mathrm{e}^{k \cdot t_0}$

2.5.2. Logarithmic Model: $A_1 + A_0 \mathrm{e}^{-k \cdot t} = a\left(1 - b\mathrm{e}^{-c \cdot t}\right)$

The logarithmic model is characterized by the constants $a = A_1$, $b = -A_0 / A_1$ and $c = k$, which influence the shape of the logarithmic curve. This curve can be described by the function $a * (1 - b \cdot \exp(-kt))$, which can be rewritten as $S(t) = A_1 - A_1 \cdot B \cdot \mathrm{e}^{-k \cdot t}$. The constant B represents the fraction of the difference between the asymptotic fineness A and the initial fineness of the powder that remains to be reached after a given grinding time. More specifically, B is equal to $((A_1 - S_0)/A_1)$, where S_0 is the initial fineness of the powder. The constant B is important because it determines how fast the fineness of the powder approaches its asymptotic fineness A_1. If the value of B is low, it means that there is a large fraction of the difference to be reached after a given grinding time, which results in a slower evolution of the fineness of the powder towards its asymptotic fineness A_1. However, this can also be advantageous in some cases.

2.5.3. Exponential-2 Model: $A_0 \mathrm{e}^{-k_0 \cdot t} + A_1 \mathrm{e}^{-k_1 \cdot t} = a + b\left(1 - \mathrm{e}^{-c \cdot t}\right) + d\left(1 - \mathrm{e}^{-e \cdot t}\right)$

The exponential-2 model relies on the constants a, b, c, d and e, which determine the shape of the double exponential curve. The process of Blaine growth as a function of grinding time can be compared to a radioactive decay with filiation. During radioactive decay, an unstable nucleus decays into a more stable nucleus by emitting particles or energy. Similarly, when grinding rocks, the large and unstable particles break into smaller and more stable particles, which results in an increase of the Blaine over the grinding time. The Blaine growth slows down with time because there are fewer large and unstable particles to fragment. This phenomenon is similar to that of radioactive decay where the number of unstable nuclei decreases as they decay, while the number of stable nuclei increases. It can be assumed that in both cases, the decay rate is independent of the complexity of the process [64] [65]. The Blaine growth model with two exponentials is described by the equation Blaine$(t) = A + A_0 \cdot \mathrm{e}^{-k_0 t} + A_1 \cdot \mathrm{e}^{-k_1 t}$. The physical constants A, A_0, A_1, k_0 and k_1 each have a particular meaning to describe the kinetics of Blaine growth. A represents the maximum value of the Blaine

achievable after an infinite grinding time, A_0 and A_1 represent the amplitude factors of the two exponentials that determine the initial and long-term growth rate, and k_0 and k_1 represent the time constants that characterize how fast the Blaine reaches its first and second peak.

2.5.4. Quadratic Model or Polynomial-2: $A_2 t^2 + A_1 t + A_0 = ct^2 + bt + a$

The constant a represented the self-crushing effect of the particles during grinding. It reflects the decrease of the specific surface Blaine increase rate with grinding time and acts as the leading coefficient of the curve. The constant $b = A_1$ represents the initial rate of increase of the specific surface Blaine, corresponding to the slope of the tangent to the graph of Blaine versus time at the origin point. The constant $c = A_2$ represents the y-intercept that corresponds to the initial Blaine. These constants allow us to characterize the kinetics of Blaine growth as a function of grinding time, using a parabolic curve to describe the relationship between the specific surface Blaine and the grinding time. The constants and statistical parameters of the models are presented in Table 8.

To fit the different mathematical models to the experimental data, we used the MATLAB Cftool tool by following the steps below:

1) We imported the data from an Excel or CSV file into MATLAB.

2) We opened Cftool by typing "Cftool" in the MATLAB command window and pressing Enter.

3) We selected "Import Data" from the "File" menu and chose the file containing our data.

4) We indicated the columns corresponding to the times and Blaine measurements in the "Import Data" window.

5) We clicked on "Create Fit" in the upper right corner of the window.

6) We chose the type of model to fit the data among the following models: the logistic function, double-component exponential, logarithmic, or quadratic polynomial.

7) We specified the model parameters, such as constants or coefficients.

8) We clicked on "Fit" to fit the model to the data.

Table 8. The constants and statistical parameters used.

Notation	Meaning
Model Constants	
A_i	Model Coefficient
K_i	Exponential Constant
Statistical parameters	
R^2	Coefficient of determination
RMSE	Root mean square error
SSE	The sum of squared errors

9) We analyzed the results of the fit to evaluate the quality of the model. We consulted the model parameters, the fit statistics and a graphical representation of the data and the fitted model.

10) If necessary, we modified the model parameters and repeated the fit until we obtained satisfactory results.

3. Results

3.1. Blaine

We measured the specific surface Blaine (SSB) of four rocks after grinding at different times. The experimental results are summarized in Tables 9-12. These tables indicate the average specific surface Blaine (SSB-average) calculated from three repetitions for each grinding time.

Table 9. Measurement of the Blaine as a function of the grinding time of the Nduizi Dolerite.

Time (min)	Bl-1 Cm²/g	Bl-2 Cm²/gr	Bl-3 Cm²/g	Average. Cm²/g
10	1378	1570	1766	1571
20	3088	3203	2778	3023
30	4134	4140	4140	4138
40	4614	4617	4639	4623
50	4895	4771	4918	4861
60	5470	5578	5474	5507
70	5995	6009	6135	6046
80	6160	6285	6260	6235

Table 10. Measurement of the Blaine as a function of the grinding time of the mainly Belitic Clinker.

Time (min)	Bl-1 Cm²/g	Bl-2 Cm²/g	Bl-3 Cm²/g	Average Cm²/g
10	996	1099	1099	1065
20	1023	1343	1496	1287
30	2015	2066	2066	2049
40	2490	2477	2464	2477
50	2781	2751	2760	2764
60	2827	3075	3080	2994
70	3067	3280	3258	3202
80	3478	3478	3480	3479
100	3632	3659	3606	3632

Table 11. Measurement of the Blaine value as a function of the grinding time of Kasi Basalt.

Time (min)	Bl-1 Cm²/g	Bl-1 Cm²/g	Bl-1 Cm²/g	Average Cm²/g
10	1760	1790	1720	1757
20	2910	2950	2870	2910
30	3760	3760	3720	3747
40	4460	4480	4420	4453
60	5040	5065	4980	5028

Table 12. Measurement of the Blaine fineness as a function of the grinding time of Matadi Metabasalt.

Time (min)	Bl-1 (cm²/g)	Bl-2 (cm²/g)	Bl-3 (cm²/g)	Average (cm²/g)
10	2090	2024	2054	2056
20	2841	2029	2432	2434
30	3345	3380	3359.5	3361.5
40	3777	3759	3765	3767
50	4127	4043	4082	4084

3.2. Statistical Parameters and Constants of the Mathematical Models

Table 13 shows the values of the statistical parameters and constants of the logistic, double exponential, logarithmic and parabolic models fitted to the experimental data on the Blaine growth. The table presents the results of fitting four mathematical models to the experimental data of the Blaine-specific surface area (SSA) as a function of the grinding time for four types of rocks. The model parameters, the coefficient of determination (R^2), the sum of squares of errors (SSE) and the root mean square error (RMSE) are given for each model and each rock. The table allows us to compare the performance of the models and to choose the most suitable one for the data. It can be observed that the two-component exponential model is the most performant for the dolerite, the clinker and the metabasalt, with the highest values of R^2 and the lowest values of SSE and RMSE.

For the basalt, the quadratic polynomial model is slightly better than the two-component exponential model. The logistic model is the least performant for all types of rocks, except for the basalt where it is comparable to the logarithmic model. The logarithmic model is also poorly performant, except for the dolerite where it is comparable to the quadratic polynomial model. According to Table 13, the two-component exponential model seems to be the most suitable for most types of rocks, as it shows the best indicators of fit quality. The quadratic polynomial model is also suitable for the basalt, where it is slightly superior to the two-component exponential model. The logistic and logarithmic models are the least suitable, as they show the worst indicators of fit quality.

Table 13. Statistical parameters and coefficients of the mathematical models used, obtained by Matlab R 2020b.

Rocks	Para.	Logarithmic	Logistic	Poly-2	Expo-2
Dolerite	A_0	1.003	4.221	580.1	3707
	A_1	6892	6217	129.8	−5141
	A_2	-	-	−0.7527	-
	k_0	0.02796	0.06296	.	0.00668
	k_1	-	-	-	−0.0759
	R^2	0.9881	0.9706	0.9807	0.9944
	SSE	2.069e+05	5.127e+05	3.375e+05	9.79e+04
	RMSE	203.4	320.2	259.7	156.5
Clinker	A_0	0.9092	3.657	538.5	10400
	A_1	4213	3696	57.83	−9968
	A_2	-	-	−0.2698	-
	k_0	0.01942	0.04811	-	−0.00402
	k_1	-	-	-	−0.01101
	R^2	0.9981	0.9939	0.9976	0.9983
	SSE	9389	30340	11820	8467
	RMSE	43.33	78.02	48.61	46.01
Metabasalt	A_0	0.7892	−2.142	1202	3334
	A_1	4896	4379	94.63	−2472
	A_2	-	-	−0.7457	-
	k_0	0.03098	0.06603	-	0.004872
	k_1	-	-	-	−0.05379
	R^2	0.9998	0.9981	0.9989	1
	SSE	592.8	4833	2753	39.56
	RMSE	17.22	49.16	37.1	6.29
Basalt	A_0	1.001	4.308	384.5	−6.057e+08
	A_1	5717	5170	148.7	+6.057e+08
	A_2	-	-	−1.188	-
	k_0	0.03612	0.08243	-	−0.01299
	k_1	-	-	-	−0.01299
	R^2	0.9984	0.9987	**0.9998**	**0.9993**
	SSE	1.06e+04	8873	1302	4752
	RMSE	72.85	66.61	**25.51**	**68.93**

3.3. Smoothing Curves with Matlab. Figure 5 Provides the Shapes of the Blaine as a Function of the Grinding Time

3.3.1. Smoothing Curves with Matlab

Figure 5 Provides the shapes of the Blaine as a function of the grinding time. The logistic and exponential functions are satisfactory for modeling the grinding
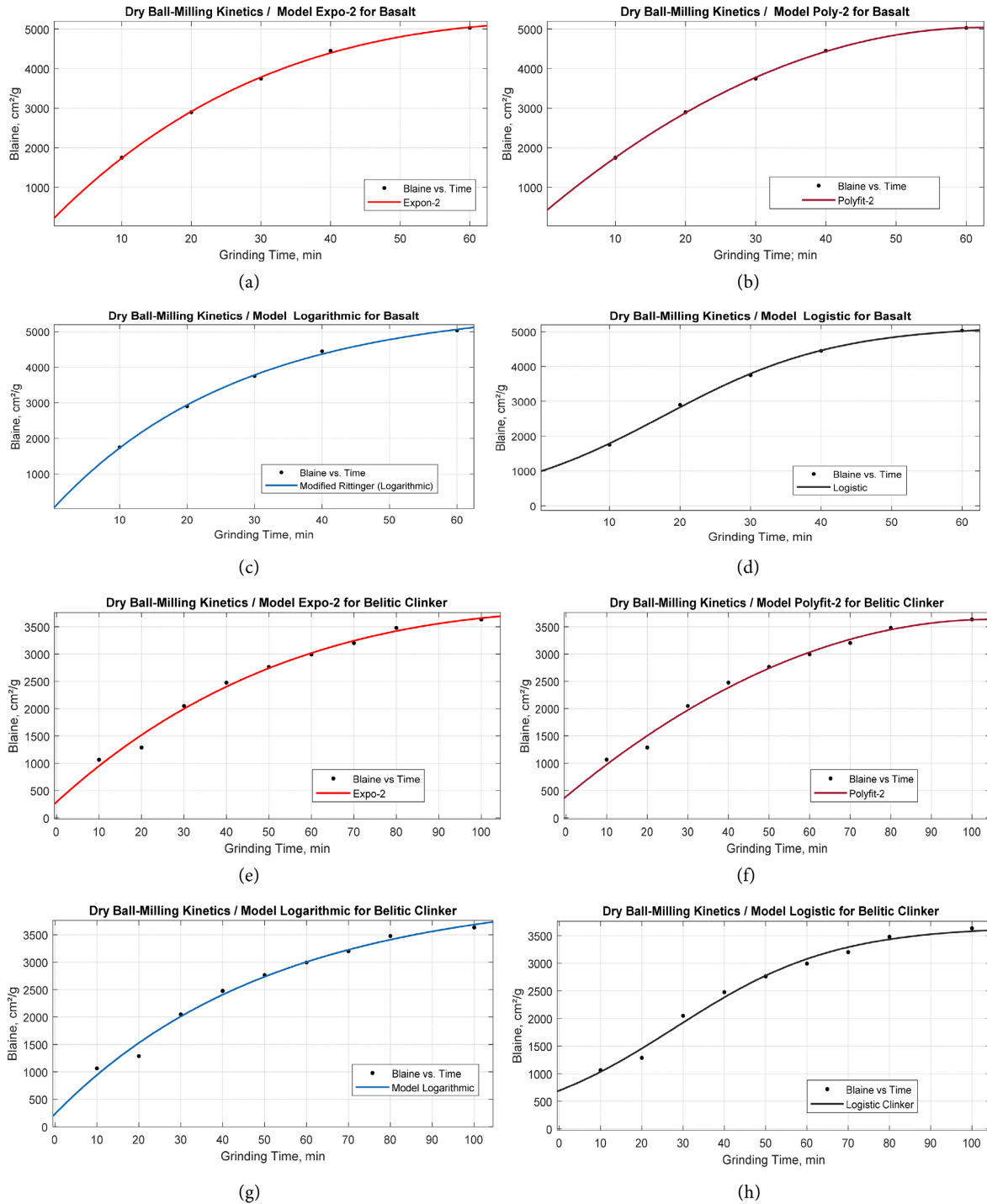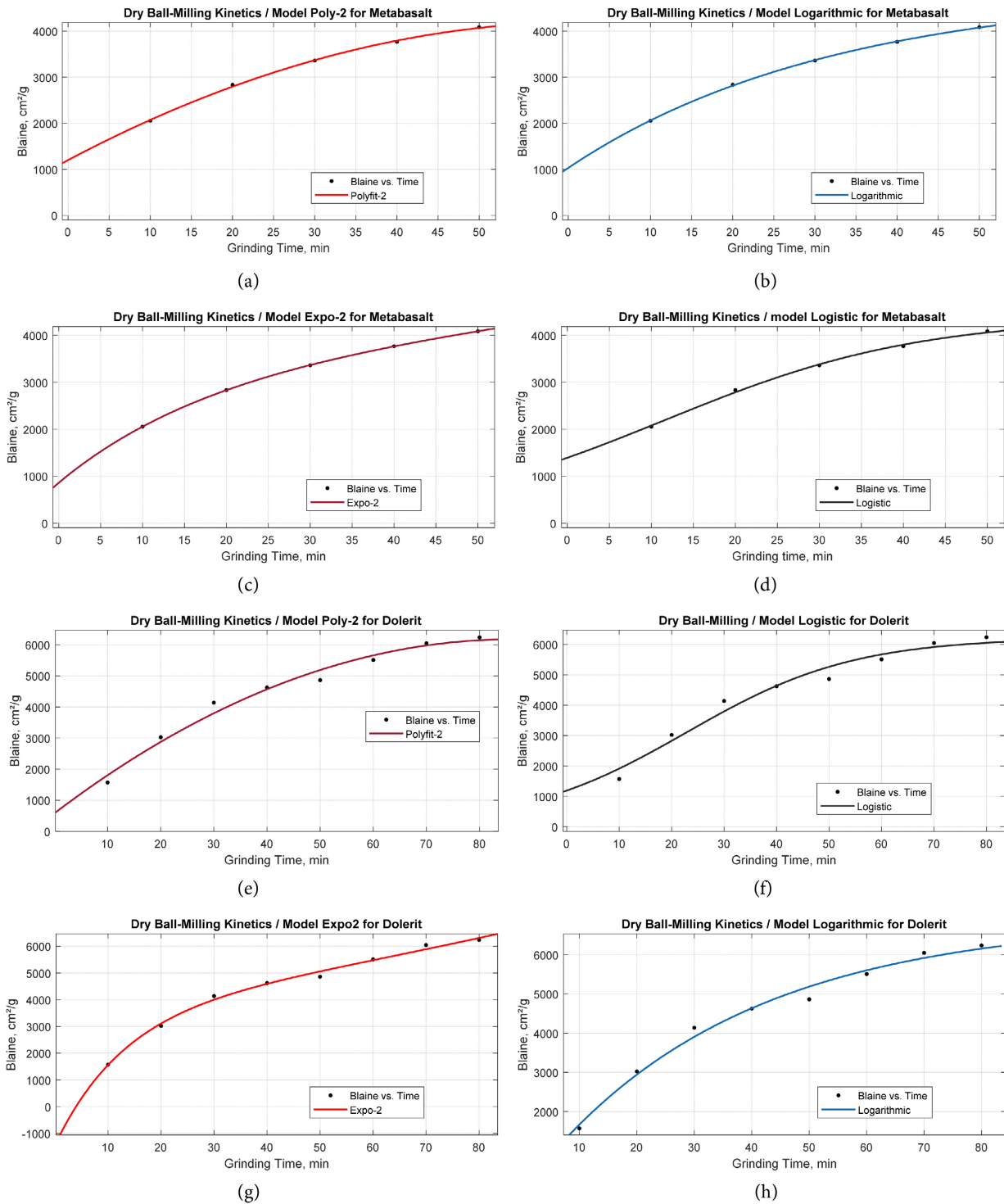

Figure 5. (a) Exponential. (d) Logistic. (b) Parabolic and (c) Logarithmic models for the Basalt, (e) Exponential, (h) Logistic, (f) Parabolic and (g) Logarithmic models for the Belitic clinker.

kinetics aiming at a given Blaine, lower or equal to the asymptotic Blaine. Compared to the parabolic functions, their ability to describe the phenomena of downward trend and re-agglomeration of particles is limited.

Figure 6 shows the same models but for the Metabasalt and the Dolerite.


Figure 6. (a) Polynomial, (b) Logarithmic, (c) Two-component exponential and (d) Logistic models for Metabasalt (e) Polynomial. (f) Logarithmic. (g) Two-component exponential and (h) Logistic models for Dolerite.

The parabolic function for the downward trend and the coupled logistic and parabolic models can be considered as more suitable in the graphical description of the phenomena of linearity according to Rittinger, agglomeration according to logistic and aggregation according to the parabola. All this is visible in the curves of **Figure 7**.

3.3.2. Comparative Curves

These curves show that this study contributes to the understanding and optimization of rock grinding in the cement industry. By observing the curves of the evolution of the Blaine obtained as a function of the type of rock and the mathematical model applied; we identify the zones of Rittinger, aggregation and agglomeration. These zones imply physical and chemical phenomena involved in the grinding of particles and determine the optimal grinding conditions for each case.


(a)

(b)

(c)

(d)
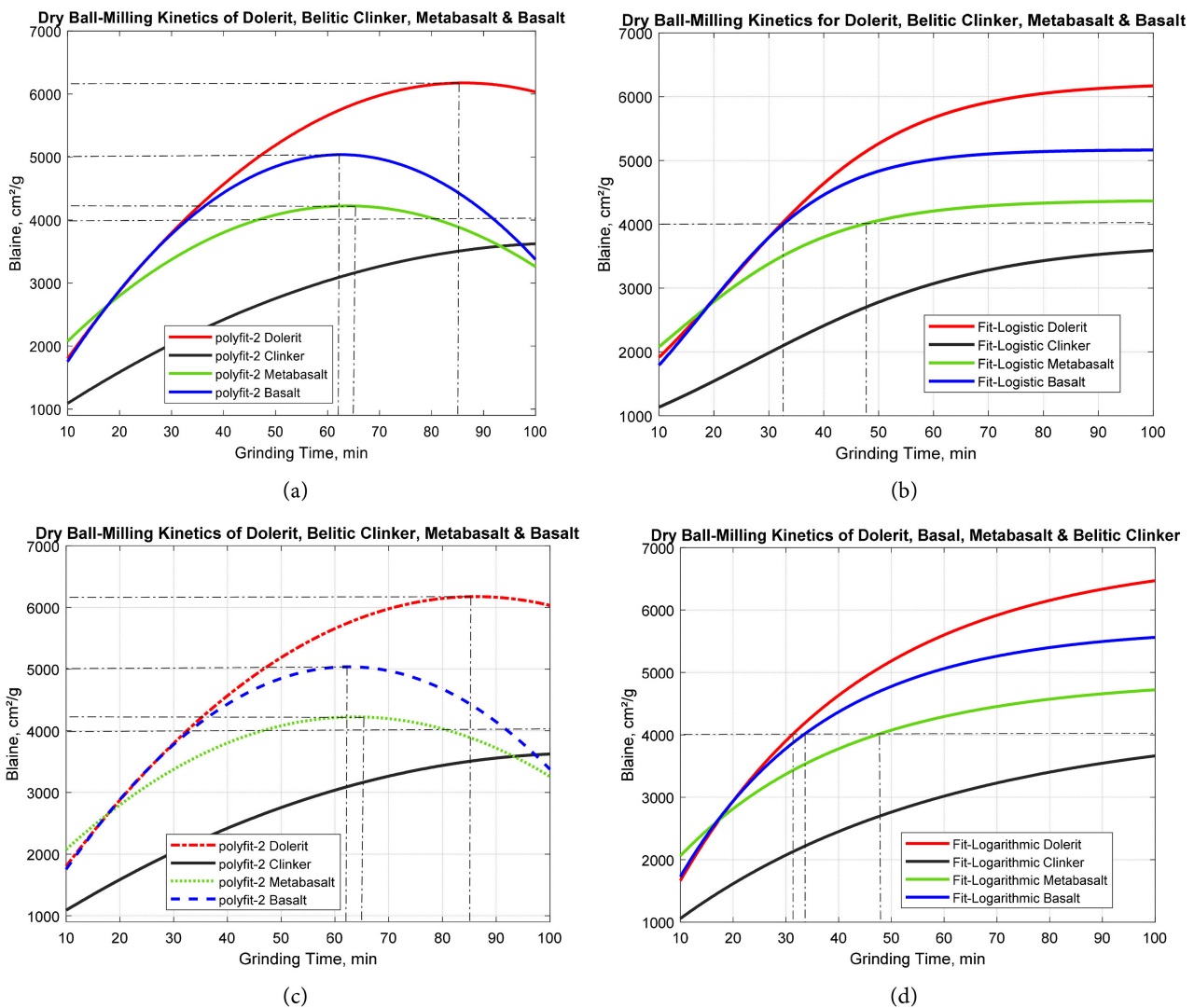
Figure 7. Comparative plot of (a) and (b) the polynomial shapes, (c) the logistic shapes, Comparative plot (d) of the logarithmic shapes.

We thus propose an improved model. This model is based on a piecewise continuous function that takes into account the two trends observed: the ascending zone up to the peak, followed by the decreasing zone of Blaine. We propose a table using the evolution of the average Blaine as a function of time obtained experimentally in the extended grinding of Clinker from **Table 14**.

- Coupled function: $S(t) = a/(1 + be^{-ct}) + (dt^2 + et + f)$,

- Logistic function: $S(t) = a/(1 + be^{-ct})$

- Piecewise continuous function:

$$S(t) = \begin{cases} \dfrac{a}{1 + b \cdot e^{-ct}} & \text{if } t \leq t_0 \\ a_1 t^2 + a_2 t + c & \text{if } t > t_0 \end{cases}$$

If we use a coupled logistic and second-order polynomial function to model the grinding of rocks, we obtain a shape whose graph is shown in **Figure 8** with the comparison of the logistic shape and the piecewise continuous one.

(a)

(b)

(c)
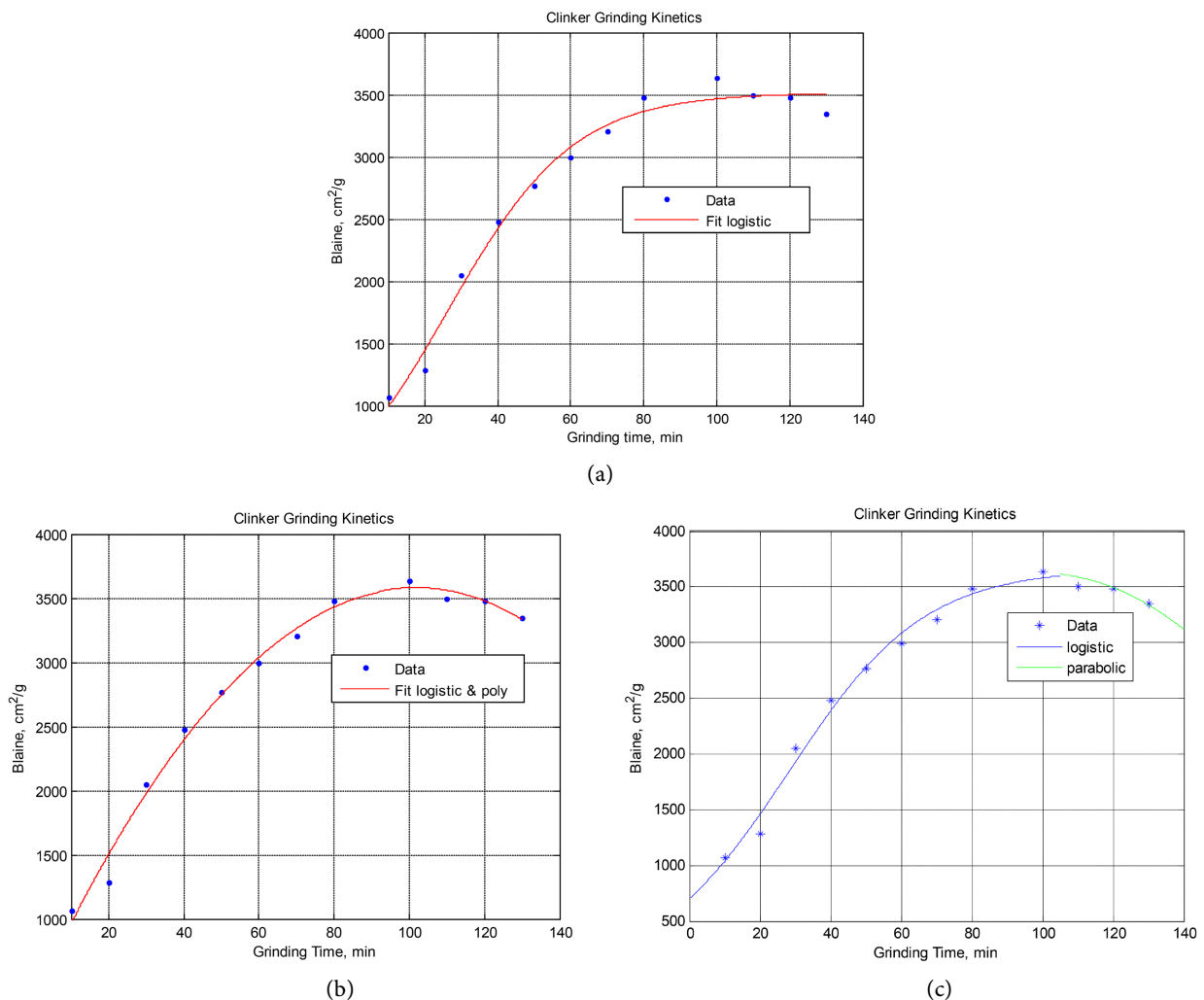
Figure 8. Fitting with (a) logistic function, (b) logistic function coupled with a second-order polynomial function and (c) the piecewise continuous function.

Table 14. Experimental data of extended grinding up to 130 minutes of grinding.

Time	10	20	30	40	50	60	70	80	100	*110*	*120*	*130*
Blaine	1065	1287	2049	2477	2764	2994	3202	3479	3632	*3500*	*3480*	*3350*

- The Logistic function:

$$S(t) = 3515.7 \big/ \left(1 + 4.5405\mathrm{e}^{-0.0577t}\right)$$

SSE = 1.2088×10^5: R^2 = 0.9859: Adj R^2 = 0.9828: RMSE = 115.8944

- The Coupled function:

$$S(t) = 183.1247 \big/ \left(1 - 22.2637\mathrm{e}^{-159.9338t}\right) + \left(-0.3090t^2 + 63.0240t + 183.7625\right)$$

SSE = 8.3438×10^4: R^2 = 0.9903: Adj R^2 = 0.9821: RMSE = 117.9252

- The piecewise continuous function:

$$S_1(t) = 3667 \big/ \left(1 + 4.2733\mathrm{e}^{-0.0518tt}\right) \quad \& \quad S_2(t) = -0.3111(tt_1 - 100)^2 + 3622.2$$

tt = 0:0.001:105 & tt_1 = 105:0.001:140

This model of piecewise continuous function helps to optimize the rock grinding process by taking into account the change of particle behavior according to the grinding time. A simple model based on a logistic, logarithmic or parabolic curve would not be accurate enough to follow this change. On the other hand, a more elaborate model based on a curve that changes shape according to the grinding time could give you more reliable and performant results.

4. Discussions

This study aimed to characterize the grinding kinetics of four types of rocks (clinker, dolerite, basalt and metabasalt) using the Blaine-specific surface area as a criterion. Four mathematical models (logarithmic, logistic, quadratic polynomial and two-component exponential) were applied to model the grinding curves and evaluate their relevance. The factor responsible for the non-linearity of the evolution of Blaine as a function of time was identified. This study highlighted the differences in grinding kinetics between four types of rocks used in the cement industry. It showed that clinker is the most resistant to grinding, which requires significant time and energy to obtain a sufficient Blaine-specific surface area. These results are in agreement with those of Benzer *et al.* [66] [67] who also observed that clinker is the most difficult material to grind among the cement components. It would therefore be interesting to study the effect of co-grinding and grinding aids on reducing the residence time and energy cost of clinker grinding, as suggested by Gao *et al.* [68]. The other rocks (dolerite, basalt and metabasalt) have faster grinding kinetics, but they are limited by a peak time beyond which grinding becomes inefficient. It would therefore be necessary to control the residence time in the mill to avoid the re-agglomeration of particles and the loss of Blaine-specific surface area [69].

These four mathematical models are then compared to fit the grinding curves and evaluate their performance. It was revealed that the two-component expo-

nential model is the most suitable for most rocks, except for the basalt which is better described by the quadratic polynomial model. The logistic and logarithmic models are the least suitable for all types of rocks. These results suggest that the grinding kinetics of particles in a mill is not linear, but follows a complex evolution that depends on the type of rock, the particle size, the comminution forces and the agglomeration phenomena induced by Van der Waals forces among others. A coupled logistic and parabolic model could be more appropriate to represent the grinding kinetics of particles, as it incorporates this inflection that underlies the different factors influencing the grinding process, as proposed by Austin *et al.* [70].

5. Conclusion and Perspectives

This study highlights the essential role of grinding granular materials in the cement industry, which allows modifying the specific surface area, the particle size distribution and the shape of the particles, which determine the physico-chemical and mechanical properties acquired by the materials. The study examines the main challenges related to the cohesion, aggregation and agglomeration of particles, which condition the performance and energy consumption of grinding. It suggests solutions adapted to the type of mill used (ball mill or horizontal mill), such as controlling the particle size, limiting the residence time, co-grinding, using grinding aids or additives, and adjusting the rotation speed of the mill or the geometry and mass of the balls. It also presents methods of optimizing the grinding process, based on the knowledge of comminution laws and interactions due to van der Waals forces, through mathematical modeling. Finally, it demonstrates the possibility of using local and reactive natural rocks as substitutes for clinker, with environmental, performance and economic benefits.

Conflicts of Interest

The authors declare that they have no known competing financial interests or personal relationships that could have appeared to influence the work reported in this paper.

Data Availability

Data will be made available on request.

References

[1] Bouzoubaa, N. and Lachemi, M. (2001) Self-Compacting Concrete Incorporating High Volumes of Class F Fly Ash: Preliminary Results. *Cement and Concrete Research*, **31**, 413-420. https://doi.org/10.1016/S0008-8846(00)00504-4

[2] Ma, J., Wang, D., Zhao, S., Duan, P. and Yang, S. (2021) Influence of Particle Morphology of Ground Fly Ash on the Fluidity and Strength of Cement Paste. *Materials*, **14**, Article 283. https://doi.org/10.3390/ma14020283

[3] Sherwani, A.F.H., Younis, K.H. and Arndt, R.W. (2022) Fresh, Mechanical, and Durability Behavior of Fly Ash-Based Self Compacted Geopolymer Concrete: Effect

of Slag Content and Various Curing Conditions. *Polymers*, **14**, Article 3209. https://doi.org/10.3390/polym14153209

[4]   Rittinger, R.P.V. (1867) Lehrbuch der Aufbereitungskunde. Ernst and Korn, Berlin.

[5]   Bond, F.C. (1952) The Third Theory of Comminution. *Transactions of the AIME*, **193**, 484-494.

[6]   Austin, L.G., Bagga, P., Celik, M. and Luckie, P.T. (1984) An Analysis of Fine Dry Grinding in Ball Mills. *Powder Technology*, **28**, 83-90. https://doi.org/10.1016/0032-5910(81)87014-3

[7]   Drahman, S.H., Kueh, A.B.H., Abidin, A.R.Z. and Nikmatin, S. (2018) Efficient Cumulative Breakage Distribution and Breakage Rate Computation with Minimal Experiment Intervention Incorporating Optimal time Determination for Fine Grinding Simulation. *Powder Technology*, **329**, 313-322. https://doi.org/10.1016/j.powtec.2018.01.075

[8]   Lee, H., Kim, K. and Lee, H. (2019) Analysis of Grinding Kinetics in a Laboratory Ball Mill Using Population-Balance-Model and Discrete-Element-Method. *Advanced Powder Technology*, **30**, 2517-2526. https://doi.org/10.1016/j.apt.2019.07.030

[9]   Zhang, W., Li, S., Song, L., Sheng, Y., Xiao, J. and Zhang, T. (2023) Studying the Effects of Varied Dosages and Grinding Times on the Mechanical Properties of Mortar. *Sustainability*, **15**, Article 5936. https://doi.org/10.3390/su15075936

[10] Krishnaraj, L. and Ravichandran, P.T. (2019) Investigation on Grinding Impact of Fly Ash Particles and Its Characterization Analysis in Cement Mortar Composites. *Ain Shams Engineering Journal*, **10**, 267-274. https://doi.org/10.1016/j.asej.2019.02.001

[11] Capece, M., Davé, R.N. and Bilgili, E. (2018) A Pseudo-Coupled DEM-Non-Linear PBM Approach for Simulating the Evolution of Particle Size during Dry Milling. *Powder Technology*, **323**, 374-384. https://doi.org/10.1016/j.powtec.2017.10.008

[12] Böttcher, A.-C., Beusen, D., Lüddecke, A., Overbeck, A., Schilde, C. and Kwade, A. (2022) Single and Multiple Breakage Events in Fine Particle Breakage Testing with a Rigidly-Mounted Roll Mill. *Minerals Engineering*, **178**, Article ID: 107390. https://doi.org/10.1016/j.mineng.2021.107390

[13] El-Shall, H. and Somasundaran, P. (1984) Physico-Chemical Aspects of Grinding: A Review of Use of Additives. *Powder Technology*, **38**, 275-293. https://doi.org/10.1016/0032-5910(84)85009-3

[14] Yekeler, M., Ozkan, A. and Austin, L.G. (2001) Kinetics of Fine Wet Grinding in a Laboratory Ball Mill. *Powder Technology*, **114**, 224-228. https://doi.org/10.1016/S0032-5910(00)00326-0

[15] Rajaonarivony, K., Rouau, X., Lampoh, K., Delenne, J.-Y. and Mayer-Laigle, C. (2019) Fine Comminution of Pine Bark: How Does Mechanical Loading Influence Particles Properties and Milling Efficiency? *Bioengineering*, **6**, Article 102. https://doi.org/10.3390/bioengineering6040102

[16] Miao, Z., Grift, T.E., Hansen, A.C. and Ting, K.C. (2011) Energy Requirement for Comminution of Biomass in Relation to Particle Physical Properties. *Industrial Crops and Products*, **33**, 504-513. https://doi.org/10.1016/j.indcrop.2010.12.016

[17] Mayer-Laigle, C., Rajaonarivony, R.K., Blanc, N. and Rouau, X. (2018) Comminution of Dry Lignocellulosic Biomass: Part II. Technologies, Improvement of Milling Performances, and Security Issues. *Bioengineering*, **5**, Article 50. https://doi.org/10.3390/bioengineering5030050

[18] Blanc, N., Mayer-Laigle, C., Frank, X., Radjai, F. and Delenne, J.-Y. (2020) Evolu-

tion of Grinding Energy and Particle Size during Dry Ball-Milling of Silica Sand. *Powder Technology*, **376**, 661-667.
https://doi.org/10.1016/j.powtec.2020.08.048

[19] Yang, J., Li, G., Yang, W. and Guan, J. (2022) Effect of Polycarboxylic Grinding Aid on Cement Chemistry and Properties. *Polymers*, **14**, Article 3905.
https://doi.org/10.3390/polym14183905

[20] Ghalandari, V. and Iranmanesh, A. (2020) Energy and Exergy Analyses for a Cement Ball Mill of a New Generation Cement Plant and Optimizing Grinding Process: A Case Study. *Advanced Powder Technology*, **31**, 1796-1810.
https://doi.org/10.1016/j.apt.2020.02.013

[21] Katsioti, M., Tsakiridis, P.E., Giannatos, P., Tsibouki, Z. and Marinos, J. (2009) Characterization of Various Cement Grinding Aids and Their Impact on Grindability and Cement Performance. *Construction and Building Materials*, **23**, 1954-1959.
https://doi.org/10.1016/j.conbuildmat.2008.09.003

[22] Nava, J.V., Llorens, T. and Menéndez-Aguado, J.M. (2020) Kinetics of Dry-Batch Grinding in a Laboratory-Scale Ball Mill of Sn-Ta-Nb Minerals from the Penouta Mine (Spain). *Metals*, **10**, Article 1687. https://doi.org/10.3390/met10121687

[23] Toprak, N. and Benzer, H. (2019) Effects of Grinding Aids on Model Parameters of a Cement Ball Mill and an Air Classifier. *Powder Technology*, **344**, 706-718.
https://doi.org/10.1016/j.powtec.2018.12.039

[24] Vargas, J.F.G., Espinosa, M., Cárdenas, Y.D., Diaz, A.H. and Martirena-Hernandez, J.F. (2020) Use of Grinding Aids for Grinding Ternary Blends Portland Cement-Calcined Clay-Limestone. In: Martirena-Hernandez, J., Alujas-Díaz, A. and Amador-Hernandez, M., Eds., *Proceedings of the International Conference of Sustainable Production and Use of Cement and Concrete*, RILEM Bookseries, Vol 22, Springer, Cham. https://doi.org/10.1007/978-3-030-22034-1_2

[25] Zunino, F. and Scrivener, K. (2021) Assessing the Effect of Alkanolamine Grinding Aids in Limestone Calcined Clay Cements Hydration. *Construction and Building Materials*, 266, Article ID: 121293.
https://doi.org/10.1016/j.conbuildmat.2020.121293

[26] Seke, V., Phuku, P., Efoto, E., Mbosei, L. and Muanda, N. (2022) Caracterisations chimique et minéralogique aux rayons X et suivi de la broyabilité des clinker, dolérite, basalte et metabasalte du Kongo-Central pour une application cimentière. *Acasti and Cedesurk Online Journal*, **10**, 11-23.

[27] Giraud, M. (2020) Analyse du comportement rhéologique des poudres à partir des propriétés des grains, application à l'étude d'un procédé de broyage/mélange pour la préparation du combustible nucléaire MOX (Doctoral dissertation). Ecole des mines d'Albi-Carmaux. https: //theses. hal. science

[28] Przlwara, P. and Kwade, A. (2020) Grinding Aids for Dry Fine Grinding Processes—Part I: Mechanism of Action and Lab-Scale Grinding. *Powder Technology*, **375**, 146-160. https://doi.org/10.1016/j.powtec.2020.07.038

[29] Matsanga, N., Nheta, W. and Chimwani, N. (2023) Grinding Media in Ball Mills-A Review. Preprints. https://doi.org/10.20944/preprints202304.0811.v1

[30] Altun, O. (2018) Energy and Cement Quality Optimization of a Cement Grinding Circuit. *Advanced Powder Technology*, **29**, 1713-1723.
https://doi.org/10.1016/j.apt.2018.04.006

[31] Ghadiri, M. and Zhang, Z.Y. (2002) Impact Attrition of Particulate Solids: Part I: A Theoretical Model of Chipping. *Chemical Engineering Science*, **57**, 3659-3669.
https://doi.org/10.1016/S0009-2509(02)00240-3

[32] Nikolić, V., García, G.G., Coello-Velázquez, A.L., Menéndez-Aguado, J.M., Trumić, M. and Trumić, M.S. (2021) A Review of Alternative Procedures to the Bond Ball Mill Standard Grindability Test. *Metals*, **11**, Article 1114. https://doi.org/10.3390/met11071114

[33] Baláž P., *et al.* (2013) Hallmarks of Mechanochemistry: From Nanoparticles to Technology. *Chemical Society Reviews*, **42**, 7571-7637. https://doi.org/10.1039/c3cs35468g

[34] Monazam, E.R., Galinsky, N.L., Breault, R.W. and Bayham, S.C. (2018) Attrition of Hematite Particles for Chemical Looping Combustion in a Conical Jet Cup. *Powder Technology*, **340**, 528-536. https://doi.org/10.1016/j.powtec.2018.09.027

[35] Chodakov, G.S. (1972) Physics of Milling. Nauka, Moscow.

[36] Alrbaihat, M., Al-Zeidaneen, F.K. and Abu-Afifeh, Q. (2022) Reviews of the Kinetics of Mechanochemistry: Theoretical and Modeling Aspects. *Materials Today*: *Proceedings*, **65**, 3651-3656. https://doi.org/10.1016/j.matpr.2022.06.195

[37] Opoczky, L. (1977) Fine Grinding and Agglomeration of Silicates. *Powder Technology*, **17**, 1-7. https://doi.org/10.1016/0032-5910(77)85037-7

[38] Chen, G.X., Li, Y.G., Liu, X. and Yang, B. (2021) Physics-Informed Bayesian Inference for Milling Stability Analysis. *International Journal of Machine Tools and Manufacture*, **167**, Article ID: 103767. https://doi.org/10.1016/j.ijmachtools.2021.103767

[39] Gábor, M. (2016) Mechanical Activation of Power Station Fly Ash by Grinding—A Review. *Journal of Silicate Based and Composite Materials*, **68**, 56-61. https://doi.org/10.14382/epitoanyag-jsbcm.2016.10

[40] Akmalaiuly, K., Berdikul, N., Pundienė, I. and Pranckevičienė, J. (2023) The Effect of Mechanical Activation of Fly Ash on Cement-Based Materials Hydration and Hardened State Properties. *Materials*, **16**, Article 2959. https://doi.org/10.3390/ma16082959

[41] Guzzo, P.L., Marinho de Barros, F.B., Soares, B.R. and Santos, J.B. (2020) Evaluation of Particle Size Reduction and Agglomeration in Dry Grinding of Natural Quartz in a Planetary Ball Mill. *Powder Technology*, **368**, 149-159. https://doi.org/10.1016/j.powtec.2020.04.052

[42] Singh, A.K. (2016) Chapter 2—Structure, Synthesis, and Application of Nanoparticles. *Engineered Nanoparticles*, 19-76. https://doi.org/10.1016/B978-0-12-801406-6.00002-9

[43] Altammar, K.A. (2023) A Review on Nanoparticles: Characteristics, Synthesis, Applications, and Challenges. *Frontiers in Microbiology*, **14**, Article ID: 1155622. https://doi.org/10.3389/fmicb.2023.1155622

[44] Fladvad, M., Onnela, T. (2020) Influence of Jaw Crusher Parameters on the Qualité of Primary Crushed Agrégats. *Minérals Engineering*, **151**, Article ID: 106338. https://doi.org/10.1016/j.mineng.2020.106338

[45] Unland, G. (2001) Assessment of the Grindability of Cement Clinker, Part 1. *Zkg International*, **54**, 61-65.

[46] Bouchenafa, O., Hamzaoui, R., Florence, C. and Mansoutre, S. (2022) Cement and Clinker Production by Indirect Mechanosynthesis Process. *Construction Materials*, **2**, 200-216. https://doi.org/10.3390/constrmater2040014

[47] Procès-verbal de laboratoire Heidelberg. (2021) LAB-QC-076-21 Analysis Report-Single sample. Analytic Center Lukala Heidelbergcement Group DRC.

[48] Price, G.D. (1993) A. Putnis *Introduction to Mineral Sciences*. Cambridge (Cam-

bridge University Press), 1992. xxii + 457 pp. Price£ 22. 95 (paperback);£ 60. 00 (hardback). *Mineralogical Magazine*, **57**, 550-551. https://doi.org/10.1180/minmag.1993.057.388.22

[49] Cornelis, K. and Philpotts, A. (2013) Philpotts. Earth Materials: Introduction to Mineralogy and Petrology. Cambridge University Press, Cambridge.

[50] Gato, J. (1972) Mineralogy, Science (Experimental). An Authorized Course of Instruction for the Quinmester Program, 25 p.

[51] Spišiak, J., Vozárová, A., Vozár, J., Ferenc, Š., Šimonová, V. and Butek, J. (2021) Implication of Mineralogy and Isotope Data on the Origin of the Permian Basic Volcanic Rocks of the Hronicum (Slovakia, Western Carpathians). *Minerals*, **11**, Article 841. https://doi.org/10.3390/min11080841

[52] Arai, S. (2019) Editorial for Special Issue "Petrology, Geochemistry and Mineralogy of the Mantle as Tools to Read Messages from the Earth's Interior". *Minerals*, **9**, Article 151. https://doi.org/10.3390/min9030151

[53] Schulz, B., Sandmann, D. and Gilbricht, S. (2020) SEM-Based Automated Mineralogy and Its Application in Geo- and Material Sciences. *Minerals*, **10**, Article 1004. https://doi.org/10.3390/min10111004

[54] Gupta, A. and Yan, D. (2016) Mineral Processing Design and Operations. 2nd Edition, Elsevier, Amsterdam, 123-152.

[55] Cisternas, L.A., Lucay, F.A. and Botero, Y.L. (2020) Trends in Modeling, Design, and Optimization of Multiphase Systems in Minerals Processing. *Minerals*, **10**, Article 22. https://doi.org/10.3390/min10010022

[56] Jean-Paul Duroudier. (2016) 4-Crushers and Grinders except Ball Mills and Rod Mills. *Size Reduction of Divided Solids*, 99-146. https://doi.org/10.1016/B978-1-78548-185-7.50004-7

[57] Austin, L.G. and Schneider, C.L. (2022) A Kinetic Model for Size Reduction in a Pilot Scale Tower Mill: Model Verification. *Minerals*, **12**, Article 679. https://doi.org/10.3390/min12060679

[58] Fuerstenau, D.W., Abouzeid, A.Z.M. and Phatak, P.B. (2010) Effect of Particulate Environment on the Kinetics and Energetics of Dry Ball Milling. *International Journal of Mineral Processing*, **97**, 52-58. https://doi.org/10.1016/j.minpro.2010.08.001

[59] Bernotat, S. and Schonert, K. (1998) Size Reduction. In: Ullmann, F. Ed., *Ullmann's Encyclopedia of sIndustrial Chemistry*. VCH Verlagsgesellschaft, Weinheim, Vol. B2, 5.1-5.39.

[60] LePree, J. (2018) Improving the Daily Grind: New Milling, Grinding and Size-Reduction Equipment Helps Processors Obtain Better Efficiencies and Develop New Products. *Chemical Engineering*, **125**, 4 p.

[61] Kalala, G.N., Chiementin, X., Rasolofondraibe, L., Boujelben, A. and Kilundu, B. (2022) Modeling Impulsive Ball Mill Forces Effects on the Dynamic Behavior of a Single-Stage Gearbox. *Machines*, **10**, Article 226. https://doi.org/10.3390/machines10040226

[62] Carman, P.C. (1937) The Determination of the Specific Surface Area of Powders I. *Journal of the Society of Chemical Industry*, **57**, 225-234.

[63] Włodarczyk-Stasiak, M. and Mazurek, A. (2021) The Use of Starch Drying Kinetics Curves for Experimental Determination of Its Specific Surface Area. *Molecules*, **26**, Article 5508. https://doi.org/10.3390/molecules26185508

[64] Hyndman, R., Koehler, A., Ord, K. and Snyder, R. (2008) Forecasting with Expo-

nential Smoothing: The State Space Approach. In: Bühlmann, P., Diggle, P., Gather, U. and Zeger, S., Eds., *Springer Science & Business Media*, Springer, Berlin. https://doi.org/10.1007/978-3-540-71918-2

[65] Shi, Y., Tang, S. and Li, J. (2020) A Two-Population Extension of the Exponential Smoothing State Space Model with a Smoothing Penalisation Scheme. *Risks*, **8**, Article 67. https://doi.org/10.3390/risks8030067

[66] Benzer, H. (2005) Modeling and Simulation of a Fully Air Swept Ball Mill in a Raw Material Grinding Circuit. *Powder Technology*, **150**, 145-154. https://doi.org/10.1016/j.powtec.2004.11.009

[67] Venkatesh, S., Ramkumar, K. and Amirtharajan, R. (2020) Predictive Controller Design for a Cement Ball Mill Grinding Process under Larger Heterogeneities in Clinker Using State-Space Models. *Designs*, **4**, Article 36. https://doi.org/10.3390/designs4030036

[68] Qin, Y.H., Han, Y.X., Gao, P., Li, Y.J. and Yuan, S. (2022) Characterization of Chalcopyrite Ore Under High Voltage Pulse Discharge: Particle Size Distribution, Fractal Dimension, Specific Energy Consumption, Grinding Kinetics. *Minerals Engineering*, **184**, Article ID: 107631. https://doi.org/10.1016/j.mineng.2022.107631

[69] Syed, F.S. (2018) Hashim and Hashim Hussin. *Journal of Physics*: *Conference Series*, **1082**, e012091. https://doi.org/10.1088/1742-6596/1082/1/012091

[70] King, R.P. (2012) Modelling and Simulation of Mineral Processing Systems. 2nd Edition, Englewood, 457 p.